Multi-view Image Restoration From Plenoptic Raw Images

Shan Xu[1], Zhi-Liang Zhou[2] and Nicholas Devaney[1]

School of Physics, National University of Ireland, Galway[1]
Academy of Opto-electronics, Chinese Academy of Sciences, Beijing[2]

Abstract. We present a reconstruction algorithm that can restore the captured 4D light field from a portable plenoptic camera without the need for calibration images. An efficient and robust estimator is proposed to accurately detect the centers of microlens images. Based on that estimator, parameters that model the centers of microlens array images are obtained by solving a global optimization problem. To further enhance the quality of reconstructed multi-view images, a novel 4D demosaicing algorithm based on kernel regression is also proposed. Our experimental results show that it outperforms the state of art algorithms.

1 Introduction

Plenoptic cameras, also known as light field cameras, are capable of capturing the radiance of light. In fact, the principle of the plenoptic camera was proposed more than a hundred years ago[1]. Thanks to the recent advances in optical fabrication and computational power, plenoptic cameras are already commercially available as a consumer commodity. There are several types of plenoptic cameras[2–5]. In this paper we focus on restoring the light field from the first consumer light field camera, the Lytro[6]. The light rays inside the camera are characterized by two planes, the exit pupil and the plane of the microlens array, which is known as two plane parametrization of 4D light field[7, 8]. Each microlens image is an image of the exit pupil viewing at different angles on the sensor plane. However, in such a spatially multiplexing device, the price to pay is the significant loss of spatial resolution. Having the 4D light field enables both novel photographic and scientific applications such as refocusing[9], changing perspective, depth estimation[10, 11] and measuring the particle's velocity in 3D [12, 13]. Evidently, these applications all rely on high quality 4D light field reconstruction.

The recent growing interest in light field imaging has resulted several papers addressing the calibration and reconstruction of the light field from a microlens-based light field camera. Donald et al.[14] proposed a decoding, calibration and rectification pipeline. Cho et al.[15] introduced a learning based interpolation algorithm to restore high quality light field images. Yunsu et al.[16] proposed a line feature based geometric calibration method for a microlens-based light field camera. All these approaches mentioned above require a uniform illuminated

image as a calibration reference image. One exception is Juliet's[9] recent work, which proposed to use dark vignetting points as a metric to find the spatial translation of microlens array respect to the center of image sensor.

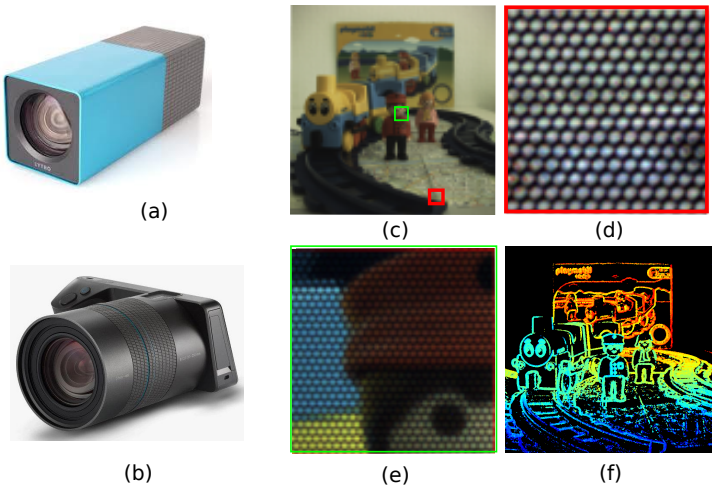

Fig. 1. (a),(b) The first and second generation Lytro cameras. (c) The microlens array raw image. (d),(e) The light field raw image (after demosaicing) with close-up views. (f) The depth estimation result from the light field raw image.

Most traditional digital color cameras use a single image sensor with a Color Filter Array (CFA)[17] on top of the senor to capture Red, Blue and Green color information. This is also a spatial-multiplexing method which gains multi-color information at the expense of losing spatial resolution. A typical light field color camera is also equipped with such a CFA sensor. The process of recovering the full color information in a single pixel is called demosaicing. Although demosaicing is a well explored topic in the image processing community, only some work has discussed demosaicing for a plentopic camera. Todor[18] proposed a demosaicing algorithm after refocusing which can reduce the color artifacts of the refocused image. Recently, Xiang et al.[19] proposed a learning based algorithm which considers the correlations between angular and spatial information. However the algorithm they proposed requires nearly an hour processing time with PC equipped with an Intel $i3-4130$ CPU.

In this paper, we present an efficient and robust processing pipeline that can restore the light field a.k.a the multi-view image array from natural light field images which doesn't need calibration images. We formulate estimating the parameters of microlens image center grid as an energy minimization problem. We also propose a novel light field demosaicing algorithm which is based on a 4D kernel regression that has been widely used in computer vision for the purpose

of de-noising, interpolation and super-resolution [20]. It is tedious to process the light field raw image taken from different cameras or even with different optical settings which all require corresponding calibration images. As our light field reconstruction algorithm is calibration file free, it simplifies the processing complexity and reduces the file storage space. Our dataset and source code are available on-line [1].

2 The Grid Model of Plenoptic Images

In this section, we derive the relation between the ideal and the practical microlens image centers which can be described by an affine transformation. In this paper, we focus on the light field camera with a microlens array placed at the focus plane of the main lens [2].

Applying a pinhole camera model to the microlenses, the center of the main lens is projected to the sensor by a microlens as shown in Fig.2(a). The microlens center (x_i', y_i') and its corresponding microlens image center (x_i, y_i) has the following geometric relation,

$$\begin{pmatrix} x_i' \\ y_i' \end{pmatrix} = \frac{Z'}{Z} \begin{pmatrix} x_i \\ y_i \end{pmatrix} \tag{1}$$

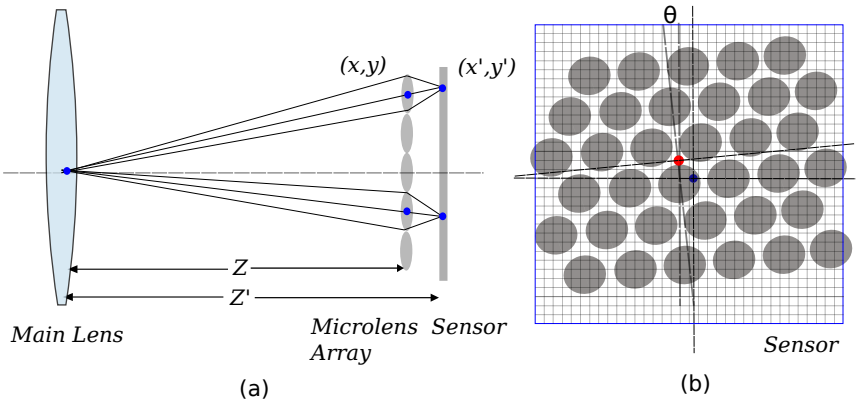

Fig. 2. (a) The main lens center is projected to sensor plane. (b) The installation errors include a ration angle θ and a translation offset $(\Delta x, \Delta y)$. The physical center of microlens array is high lighted in red and the physical center of sensor is high lighted in blue.

Ideally, the microlens array has perfect regular arrangement such as a square or hexagonal grid. Nevertheless, the manufacturing error and installation error can be observed in the raw images. The lateral skew parameters σ_1,σ_2 ,the

[1] https://sites.google.com/site/lfmulview

rotation angle θ and the translation parameters T_x,T_y are considered as the main sources of position displacement. If we use s to substitute $\frac{Z'}{Z}$ in Eq.1, and approximate $sin\theta = \epsilon, cos\theta = 1$ as the rotation is tiny, we obtain,

$$\begin{pmatrix} x' \\ y' \\ 1 \end{pmatrix} = s \begin{pmatrix} 1 & \epsilon & 0 \\ -\epsilon & 1 & 0 \\ 0 & 0 & 1 \end{pmatrix} \cdot \begin{pmatrix} 1 & \sigma_1 & T_x \\ \sigma_2 & 1 & T_y \\ 0 & 0 & 1 \end{pmatrix} \cdot \begin{pmatrix} x \\ y \\ 1 \end{pmatrix} = s \begin{pmatrix} \sigma_2 - \epsilon & \sigma_2\epsilon + 1 & Tx \\ \sigma_1 - \epsilon & \sigma_1\epsilon + 1 & Ty \\ 0 & 0 & 1 \end{pmatrix} \cdot \begin{pmatrix} x \\ y \\ 1 \end{pmatrix} \tag{2}$$

Equation (2) shows that the relation between the microlens center (x_i, y_i) and its image center (x'_i, y'_i) can be expressed by an affine transform with six parameters. The above derivation explains why an affine transform matrix is preferred as a good transformation model to be used for estimating the centers of the microlens array.

3 Multi-view Images Restoration Algorithm

In decoding the 4D light field a.k.a extract the multi-view image array from a 2D raw image, the center of each microlens image is regarded as the origin of embedded 2D data. To accurately detect the position of each microlens image is the fundamental step of restoring high quality light field. We first introduce a robust local centroiding estimator which is insensitive to the content and shape of microlens image compared to conventional centroiding estimators. Next, we formulate estimating the grid parameters problem in terms of energy minimization. We break our brute-force search algorithm into three steps to reduce the processing time. In the last section, a 4D demosaicing algorithm is exploited to improve the quality of the reconstructed images.

3.1 Local Centroiding Estimator

In Cho et al's. and Dansereau et al.'s papers [14, 15], the center of each microlens image is determined either by convolving a 2D filter or performing an eroding operation from the uniform illumination light field raw image. However, the limitation of previous methods is that the image needs to be uniform and in a circular shape. In practice, some microlens images are distorted by vignetting effect[21] and the Bayer filter makes the image less uniform. In contrast, we measure the individual microlens image centers by examining the dark pixels among the microlens images. Concretely, for either a square or hexagonal microlens array, there are dark gaps between microlens images. For example, as shown in Fig.3, the position of the darkest spots of a hexagonal grid with respect to the center of a microlens are $\boldsymbol{p_0} = (R, \frac{R}{\sqrt{3}})$, $\boldsymbol{p_1} = (0, \frac{2R}{\sqrt{3}})$, $\boldsymbol{p_2} = (-R, \frac{R}{\sqrt{3}})$, $\boldsymbol{p_3} = (-R, -\frac{R}{\sqrt{3}})$, $\boldsymbol{p_4} = (0, -\frac{2R}{\sqrt{3}})$, $\boldsymbol{p_5} = (R, -\frac{R}{\sqrt{3}})$, where R is the radius of the hexagonal grid. For an arbitrary pixel at position $\boldsymbol{x} = [x, y]^T$ of the light field raw image I, the summation of the six special surrounding pixels denoted by

$P(\boldsymbol{x})$ is used for detecting the center of the microlens image. To achieve sub-pixel accuracy, we up-sample the image by a factor of 8 with cubic interpolation. Additionally, to reduce the effect of dark current, a Gaussian filter is applied before the up-sampling. The local centroiding estimator is defined as a score map $\mathcal{P}(\boldsymbol{x})$,

$$\mathcal{P}(\boldsymbol{x}) = \boldsymbol{\Sigma}_{i=0}^{5}(G_\sigma * I_{\uparrow 8})(\boldsymbol{x} + \boldsymbol{p_i}) \tag{3}$$

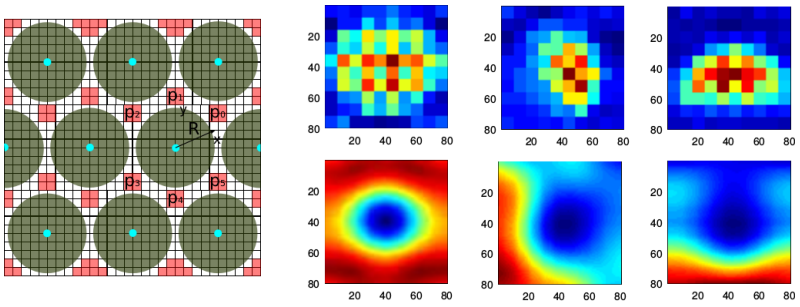

Fig. 3. Left: The hexagonal grid microlens array image. The dark gap pixels are labeled in pink. Right: top row are the microlens images with different shapes. Bottom row are our local estimator score maps $\mathcal{P}$.

If the light field raw image is uniformly illuminated, $P(\boldsymbol{x})$ reaches a minimum only when $\boldsymbol{x}$ is at the center of a microlens image. The nice property of this operator is that it constantly produces minimum when $\boldsymbol{x}$ is the center of a microlens image regardless of its content. Notice that, if there some under-exposed pixels inside surrounding microlens images, the multiple minimum points may exist. The center point $\boldsymbol{x}_{center}$ belongs to the minimum points set,

$$\boldsymbol{x}_{center} \in \{\boldsymbol{x}_i | \mathcal{P}(\boldsymbol{x}_i) = \mathcal{P}_{min}, i = 0, ...N\} \tag{4}$$

Evidently, our local estimator is not able to find all the microlens image centers from a natural light field raw image individually. In the next section, instead of using the local minimum to identify the individual microlens image center, we propose a global optimization scheme to estimate the global grid parameters.

3.2 Global Grid Parameters Optimization

For a natural scene, it is impractical to accurately measure the centers of those microlens images that are under-exposed or over-exposed. As a consequence, estimating the transformation matrix [22] by the method of minimizing Euclidean distance between the ideal and real point set is not applicable to this problem.

Our approach first generates an up-sampled centroiding score map $\mathcal{P}$ based on our local estimators. Then we can use the summation of all pixels on the grid as a metric to measure how well is the grid fitted to the centers of the microlens array. As shown in Fig.4, only a best fitted grid model will produce the global minimum.

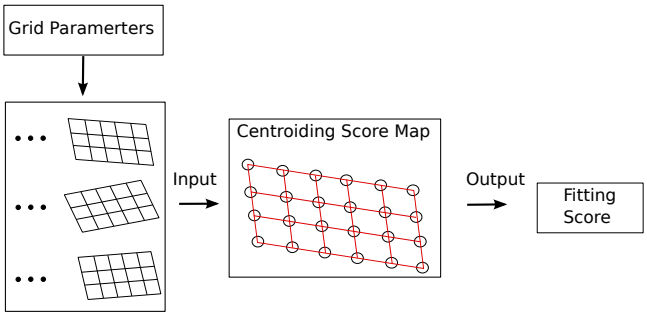

Fig. 4. Grid Fitting. Only when the grid parameters are all optimum, the fitting score reaches minimum as highlighted in red color.

Thus we formulate it as a global optimization problem. The cost function $\mathcal{F}$ is defined as,

$$\boldsymbol{\mathcal{F}}(s, \sigma_1, \sigma_2, \epsilon, Tx, Ty) = \boldsymbol{\Sigma}_{j=1}^{M} \Sigma_{i=1}^{N} \boldsymbol{\mathcal{P}}(\boldsymbol{\mathcal{T}}(s, \sigma_1, \sigma_2, \epsilon, Tx, Ty) \cdot \boldsymbol{x}_{ji}) \tag{5}$$

where $\boldsymbol{x}_{ij} = [x_{ij}, y_{ij}]^T$ is the spatial position of ijth microlens center and $\mathcal{T}$ is the homogeneous affine transformation which matrix form given in Eq.1. The cost function $\mathcal{F}$ reaches a global minimum only when the grid parameters are accurately estimated.

In our experiment, several numerical optimization methods have been applied to solve this problem. For example, the NelderMead algorithm[23] has fast convergence rates but occasionally gets stuck at a local minimum. The simulated annealing algorithm [24] as a probabilistic method guarantees the solution is a global minimum but the rate of convergence is very slow. Also tuning the parameters such as the cooling factor can be troublesome. Considering there are only small affine transformation between practical and ideal microlens image centers, we perform a coarse-to-fine brute-force searching scheme. The perfect microlens center grid $\{\boldsymbol{x}_{ji} | i = 0 \cdots N, j = 0 \cdots N\}$ is used as the initial condition and is constructed based on the geometric arrangement of the microlens array. We assume the physical separation between microlenses d and pixel size l are known parameters. For a hexagonal grid microlens array, we have,

$$\boldsymbol{x}_{ji} = \begin{cases} (i \cdot \frac{d}{l}, j \cdot \frac{\sqrt{3}d}{l}) & \text{for j is odd} \\ (i \cdot \frac{d}{l}, j \cdot \frac{\sqrt{3}d}{l}) - (\frac{d}{2}, \frac{\sqrt{3}d}{2}) & \text{for j is even} \end{cases} \tag{6}$$

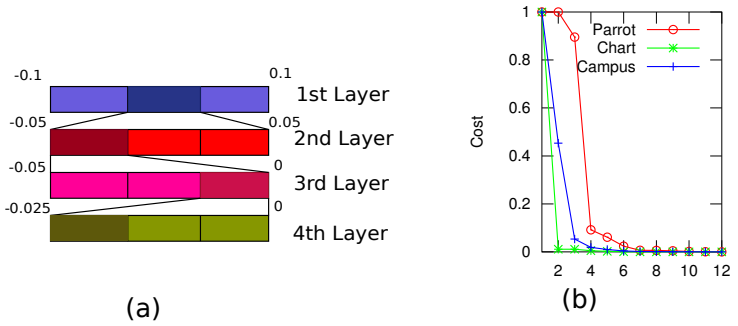

Fig. 5. (a) Sketch of our coarse-to-fine searching algorithm. The sub-region highlighted in dark color is the optimal parameter at current layer's resolution.(b) The cost function converges within 8 iterations. Three scenes were captured with different Lytro cameras.

To speed up the searching, we set reasonable boundary constrains for each parameter. The spatial translation T_x and T_y are in the range of $[-\frac{d}{2l}, \frac{d}{2l}]$. We also assume the rotation and skew angle is within ± 0.1 degree. To search the parameter in 6 dimensions will be time consuming. We divide it into three steps: we first search T_x and T_y then $s, \sigma_1, \sigma_2, \epsilon$ and finally refine T_x and T_y. Each step includes several searches with different resolution as illustrated in Fig.5(a). For each search, the optimal solution from the previous search is used as the searching center, and the searching range is narrow downed by one half. Fig.5(b) shows that with different scenes and cameras, our proposed algorithm has fast convergence. We summarize the algorithm as follows in Tab.1.

As mentioned above, for a natural light field image, some parts of microlens images or entire microlens images might be under-exposed and this might influence the accuracy of our proposed algorithm. However, our experiment shows that the under-exposure effect only has minor impact on the estimation accuracy. We compare the microlens image centers estimated from the white uniform illumination scene and a natural scene with same optical settings. The largest error is within half a pixel and it occurs only when there are large under-exposed regions.

3.3 4D Light Field Demosaicing

Applying a conventional 2D demosaicing algorithm to the light field raw images produces noticeable color artifacts. The reason is pixels on the boundary of

Input : Centroiding score map $\mathcal{P}$
Output : Optimum parameters $s_0, \sigma_{10}, \sigma_{20}, \epsilon_0, Tx_0, Ty_0$

Processing:
Step 0. Parameter initialization $s_0, \sigma_{10}, \sigma_{20}, \epsilon_0, Tx_0, Ty_0$.
Step 1. 2D search to find optimum Tx and Ty.
for $k \leftarrow 0$ **to** K **do**
  for $j \leftarrow -N$ **to** N **do**
    for $i \leftarrow -N$ **to** N **do**
      $Tx_i = Tx_0 + \delta x \cdot i$
      $Ty_i = Ty_0 + \delta x \cdot j$
      Update $\mathcal{F}$
      if $\mathcal{F} < \mathcal{F}_{min}$ **then** $\mathcal{F}_{min} \leftarrow \mathcal{F}$, $T_x = Tx_i, T_y = Ty_j$;
      ;
    end
  end
  Scale down the searching range to $[-\frac{N}{K^k}, \frac{N}{K^k}]$.
end
Step 2. 4D search for finding optimum $s, \sigma_1, \sigma_2, \epsilon$.
Update $s, \sigma_1, \sigma_2, \epsilon$ similar to Step 1.
Step 3. Refine optimum Tx, Ty similar to Step 1.

Algorithm 1: Brute-Force coarse-to-fine Searching

Table 1. Grid Modeling Prediction Error

	ISO chart	Campus	Parrot	Toy	Flower
$l2-$**norm**	0.014	0.333	0.246	0.151	0.490

Fig. 6. Test Scene. (a) ISO chart. (b) Campus. (c) Parrot. (d) Toy. (e) Flower.

microlens image are interpolated with the pixels from adjacent microlens images which are not their 4D neighbors. Intuitively, in contrast to 2D demosaicing, 4D demosaicing should result in better quality if the coherence of both angular and spatial information is considered. In order to infer the interest pixel value from the structure of its 4D neighbors, we use the first order 4D kernel regression method. Concretely, borrowing the notation from [20], the local 4D function $f(\boldsymbol{x})$, $\boldsymbol{x} \in \mathbb{R}^4$ at a given sample point $\boldsymbol{x_i}$, can be expressed by Taylor expansion,

$$f(\boldsymbol{x_i}) = f(\boldsymbol{x}) + (\boldsymbol{x} - \boldsymbol{x_i})^T \nabla f(\boldsymbol{x}) + \cdots \tag{7}$$

where $\nabla f(\boldsymbol{x}) = [\frac{\partial f(\boldsymbol{x})}{\partial x_0}, \frac{\partial f(\boldsymbol{x})}{\partial x_1}, \frac{\partial f(\boldsymbol{x})}{\partial x_2}, \frac{\partial f(\boldsymbol{x})}{\partial x_3}]^T$
Equation (7) can be converted to a linear filtering formula,

$$f(\boldsymbol{x_i}) \approx \beta_0 + \boldsymbol{\beta}_1^T(\boldsymbol{x} - \boldsymbol{x_i}) \tag{8}$$

where $\beta_0 = f(\boldsymbol{x})$, $\boldsymbol{\beta}_1 = [\frac{\partial f(\boldsymbol{x})}{\partial x_0}, \frac{\partial f(\boldsymbol{x})}{\partial x_1}, \frac{\partial f(\boldsymbol{x})}{\partial x_2}, \frac{\partial f(\boldsymbol{x})}{\partial x_3}]^T$,

Therefore a 4D light field demosaicing problem is the estimation of an unknown pixel $\boldsymbol{x}$ from a measured irregularly sampled data set $\{\boldsymbol{x_i} \in \mathbb{R}^4 | i = 1, \ldots, N\}$. The solution is a weighted least squares problem, in the form,

$$\hat{\boldsymbol{b}} = \underset{\boldsymbol{b}}{\operatorname{argmin}} (\boldsymbol{y} - \boldsymbol{X}\boldsymbol{b})^T \boldsymbol{K} (\boldsymbol{y} - \boldsymbol{X}\boldsymbol{b}) \tag{9}$$

where $\boldsymbol{y} = [f_1, f_2, \ldots, f_N]^T$,$\boldsymbol{b} = [\beta_0, \boldsymbol{\beta}_1^T]$, $\boldsymbol{X} = \begin{bmatrix} 1 & \boldsymbol{x} - \boldsymbol{x_1} \\ 1 & \boldsymbol{x} - \boldsymbol{x_2} \\ \vdots & \vdots \\ 1 & \boldsymbol{x} - \boldsymbol{x_N} \end{bmatrix}$
$\boldsymbol{K} = diag[K(\boldsymbol{x} - \boldsymbol{x_0}), K(\boldsymbol{x} - \boldsymbol{x_1}), K(\boldsymbol{x} - \boldsymbol{x_2}), \cdots, K(\boldsymbol{x} - \boldsymbol{x_{N-1}})]$
The detailed derivation of the above formulas in N-dimensions can be found in [20]. We use a Gaussian function as the Kernel function and only the pixels which within the distance of 2 pixels are included in the sample data set in each dimension. In the experimental results section, we compare the demosaicing result with our proposed algorithm, 4D-quad-linear interpolation method and 2D demosaicing method.

3.4 Mult-view Reconstruction Pipeline

A plentoptic camera processing pipeline is shown in Fig.7. Note that our processing pipeline only requires light field raw images.

4 Experimental Result

Our experiment is based on the first commercially available consumer light field camera, the Lytro[6]. It has approximately 360 by 380 microlenses. There are around 10 by 10 pixels under each individual microlens. The resolution of the image sensor is 3,280 x 3,280 pixels. To avoid aliasing of boundary pixels of the microlens image, we extract a 9 by 9 multi-view array. Our light field reconstruction algorithm is implemented in C++. It takes around 1 minutes to build the grid model and 8 minutes to extract the whole multiview array images with an Intel $i3-4130$ CPU.

To verify our 4D demosaicing algorithm, in Fig.8 we compare our method with traditional 2D demosaicing and 4D quad-linear interpolation method. The result from 2D demosaicing looks sharper but also contains much more color artifacts than our result. The result from 4D demosaicing has the fewest color artifacts, but it is too blurry as each pixel is interpolated with surrounding pixels

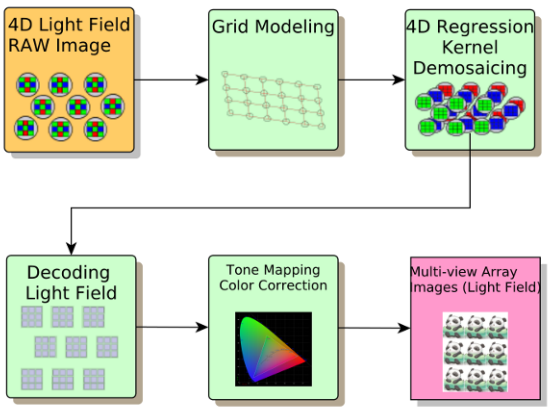

Fig. 7. Our proposed plentoptic camera processing pipeline

with weight proportional to the distance without considering the underlying data structure.

In Fig.9 we also compare our reconstructed multiview image with Dansereau et al.'s[14] and Cho et al.'s[15] results. They reconstructed the images using both light field raw image and calibration image, but we only process the light field raw images. We didn't compare Cho et al.'s result after dictionary learning as our purpose is to reconstruct the light field image with the single raw image. From the comparison, our results produce less artifacts and are less noisy than both their results.

5 Conclusion

In this paper, we have presented a simple and efficient method that is able to reconstruct the light field from the natural light field raw image without the need for reference images. To accurately extract 4D light field data from 2D light field raw image, the parameters of the grid model of microlens array are optimized by solving a global optimization problem. We describe our detailed implementation of coarse-to-fine brute force search. We also demonstrate that the content inside the microlens image has only minor impact on the accuracy of the grid model. For the purpose of further improving the quality of the reconstructed light field, a 4D demosaicing algorithm is introduced. In our further work, we plan to include vignetting correction and geometry distortion correction into our light field processing pipeline.

References

1. Gabriel, L.: La photographie intégrale. Comptes-Rendus, Académie des Sciences **146** (1908) 446–551

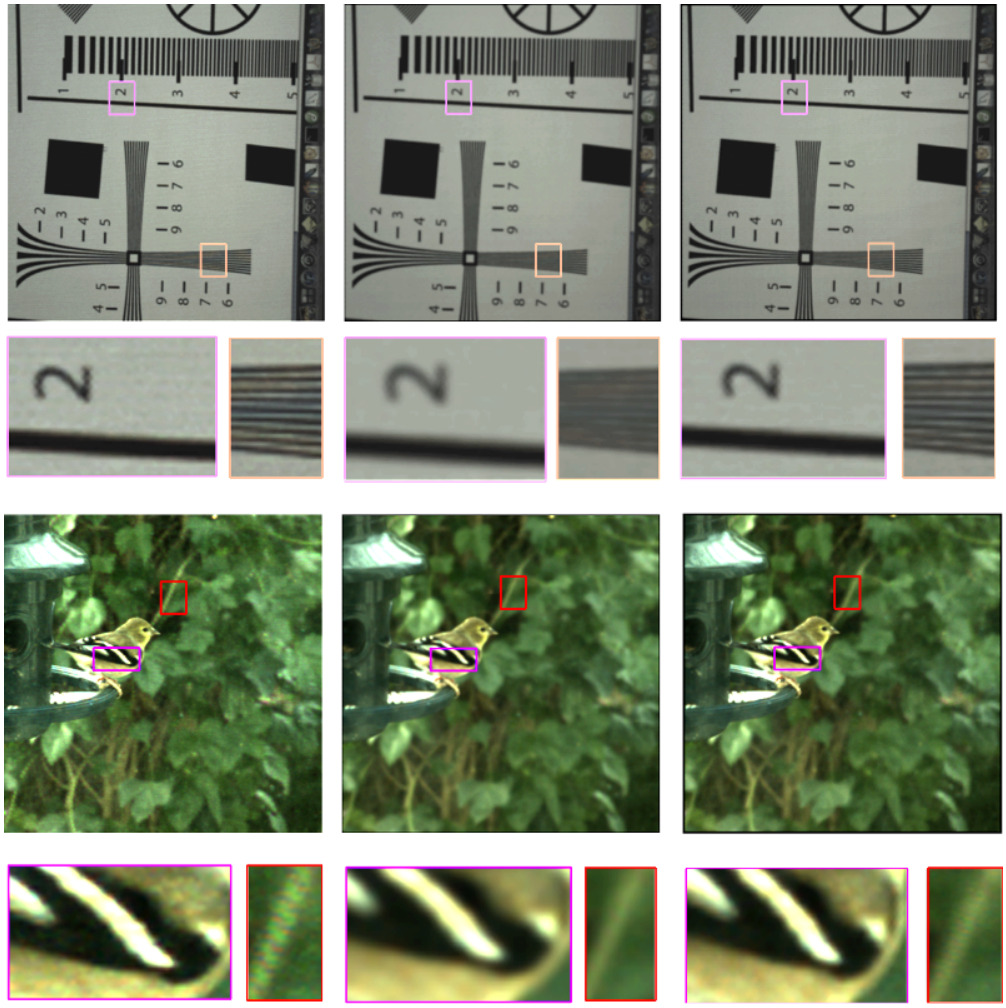

Fig. 8. Demosaicinge examples using real world examples. Left column: 2D demosaicing. Central column: 4D quad-llinear demosaicing. Right column: 4D kernel regression demosaicing.

2. Ng, R., Levoy, M., Brédif, M., Duval, G., Horowitz, M., Hanrahan, P.: Light Field Photography with a Hand-Held Plenoptic Camera. Technical report (2005)
3. Lumsdaine, A., Georgiev, T.: Full resolution lightfield rendering. Technical report, Adobe (2008)
4. Veeraraghavan, A., Raskar, R., Agrawal, A., Mohan, A., Tumblin, J.: Dappled photography: Mask enhanced cameras for heterodyned light fields and coded aperture refocusing. SIGGRAPH **26** (2007)
5. Liang, C.K., Lin, T.H., Wong, B.Y., Liu, C., Chen, H.: Programmable aperture photography: Multiplexed light field acquisition. SIGGRAPH **27** (2008) 55:1–55:10

Fig. 9. Top row: left is Don et al.'s[14] result, right is our result. Bottom row: left is Cho et al.'s[15] result, right is our result. The image is the central view cropped from the reconstructed multiview light field image.

6. Todor Georgiev, Zhan Yu, A.L.S.G.: Lytro camera technology: Theory, algorithms, performance analysis. In: MCP, SPIE (2013)

7. Levoy, M., Hanrahan, P.: Light field rendering. SIGGRAPH (1996) 31–42

8. Gortler, S.J., Grzeszczuk, R., Szeliski, R., Cohen, M.F.: The lumigraph. SIGGRAPH (1996) 43–54
9. Fiss, J., Curless, B., Szeliski, R.: Refocusing plenoptic images using depth-adaptive splatting. (2014)
10. Tao, M.W., Hadap, S., Malik, J., Ramamoorthi, R.: Depth from combining defocus and correspondence using light-field cameras. (2013)
11. Yu, Z., Guo, X., Ling, H., Lumsdaine, A., Yu, J.: Line assisted light field triangulation and stereo matching. In: ICCV, IEEE (2013)
12. Lynch, K., Fahringer, T., Thurow, B.: Three-dimensional particle image velocimetry using a plenoptic camera. 50th AIAA Aerospace Sciences Meeting including the New Horizons Forum and Aerospace Exposition (2012)
13. Garbe, C.S., Voss, B., Stapf, J.: Plenoptic particle streak velocimetry (ppsv): 3d3c fluid flow measurement from light fields with a single plenoptic camera. 16th Int Symp on Applications of Laser Techniques to Fluid Mechanics (2012)
14. Dansereau, D.G., Pizarro, O., Williams, S.B.: Decoding, calibration and rectification for lenselet-based plenoptic cameras. In: CVPR, IEEE (2013)
15. Cho, D., Lee, M., Kim, S., Tai, Y.W.: Modeling the calibration pipeline of the lytro camera for high quality light-field image reconstruction. In: ICCV, IEEE (2013)
16. Yunsu Bok, H.G.J., Kweon, I.S.: Geometric calibration of micro-lens-based light-field cameras using line features. In: ICCV, IEEE (2014)
17. Bayer, B.E.: Color image array. (1976)
18. Georgiev, T.: An analysis of color demosaicing in plenoptic cameras. In: Proceedings of the 2012 IEEE Conference on Computer Vision and Pattern Recognition (CVPR). CVPR '12, Washington, DC, USA, IEEE Computer Society (2012) 901–908
19. Xiang Huang, O.C.: Dictionary learning based color demosaicing for plenoptic cameras. In: ICCV, IEEE (2013)
20. Takeda, H., Farsiu, S., Milanfar, P.: Kernel regression for image processing and reconstruction. IEEE TRANSACTIONS ON IMAGE PROCESSING **16** (2007) 349–366
21. Xu, S., Devaney, N.: Vignetting modeling and correction for a microlens-based light field camera. IMVIP (2014)
22. Sabater, N., Drazic, V., Seifi, M., Sandri, G., Perez, P.: Light-field demultiplexing and disparity estimation. (2014)
23. Nelder, J.A., Mead, R.: A simplex method for function minimization. Computer Journal (1965) 308–313
24. Kirkpatrick, S., Gelatt, C.D., Vecchi, M.P.: Optimization by simulated annealing. SCIENCE **220** (1983) 671–680